Path integral description of low-dimensional polarons in parabolic confinement potentials

1997 J. Phys.: Condens. Matter 9 5067

(http://iopscience.iop.org/0953-8984/9/24/007)

J. Phys.: Condens. Matter **9** (1997) 5067–5079. Printed in the UK PII: S0953-8984(97)80631-5

Path integral description of low-dimensional polarons in parabolic confinement potentials

R T Senger and A Erçelebi

Department of Physics, Bilkent University, 06533 Ankara, Turkey

Received 3 January 1997, in final form 18 March 1997

Abstract. Within the framework of the Feynman path integral theory, we provide a unified insight into ground-state properties of the Fröhlich polaron in low-dimensionally confined media. The model that we adopt consists of an electron immersed in the field of bulk LO phonons and bounded within an anisotropic parabolic potential box, whose barrier slopes can be tuned so as to yield an explicit tracking of the Fröhlich interaction encompassing the bulk and all low-dimensional geometric configurations of general interest.

1. Introduction

In the last two decades, considerable interest has developed in the study of polarons in low-dimensionally confined quantum systems. The common theoretical prediction concluded by the relevant work in the literature is that the electron couples more efficiently to the phonons with increasing degree of confinement, and, consequently, certain polaron quantities scale to rather pronounced values above their bulk values. The ground-state energy, for instance, becomes lowered by a factor of $\pi/2$ ($\frac{3}{8}\pi^2$) below its corresponding bulk value for weak (strong) coupling as the dimensionality is reduced from three to two [1, 2]. For systems of even lower dimensionality, namely quasi-one-dimensional (Q1D) quantum well wires, the polaron binding is even deeper, with much stronger electron–phonon coupling than in comparable quasi-two-dimensional (Q2D) quantum well structures [3, 4]. Going on further to confinement geometries squeezing the electronic density in all directions, such as is found, for instance, in zero-dimensional (Q0D) quantum-box-type configurations, the pseudo-enhancement in the effective electron–phonon coupling can be much more sturdy than for the two- or one-dimensional cases.

One remark that we might make in this regard is that high degrees of localization in reduced dimensionalities give rise to the possibility that, in spite of a weak polar coupling, like that in GaAs for instance, the polaron problem may show a strong-coupling aspect stemming from confinement effects. This salient feature can be more prominent in II–VI compound semiconductors or in alkali halides, where the relevant coupling strengths are almost an order of magnitude larger or even much stronger than those for III–V compounds. We thus feel that for electron–phonon couplings that are not too weak and/or are pseudo-enhanced, a pure perturbation treatment of the polaron Hamiltonian may not be entirely appropriate. We were therefore encouraged to formulate the confined-polaron problem within the framework of the Feynman path integral theory [5], which proves to be a convenient and powerful technique in the treatment of the Fröhlich interaction over the entire ranges of the electron–phonon coupling strength and the degree of confinement.

0953-8984/97/245067+13$19.50

A description of the lowest polaron bound state within a generalized confining potential, which can be tuned to all geometric configurations and interesting regimes of the effective dimensionality, has already been reviewed by Yıldırım and one of the present authors [6, 7]. However, the relevant discussions were restricted to either the strong- or the weak-coupling limit. In what follows we refer to the same model as was used in these papers, and present a means of formulating the problem somewhat differently by utilizing the Feynman path integral technique, thus enabling us to provide a wider, comprehensive insight into polaron properties in confined media with arbitrary electron–phonon coupling strength.

In the foregoing theory, a low-dimensionally confined electron, assuming a simple situation—namely an anisotropic potential box with adjustable parabolic barriers—was considered. The composite assembly will thus be visualized as immersed in a bosonic reservoir where the electron couples to the LO branch of the bulk phonon spectrum. Hence, the fundamental approach followed in this work is to take into account solely the generic low-dimensional aspect of the dynamical behaviour of the electron, and to leave out all of the other effects; thus, we focus our concern primarily on giving a clear view of just the bulk phonon effects in confined media. Apart from ignoring the contributions that may arise from all of the other kinds of phonon mode, we also omit the screening effects and further detailed features, such as those due to the non-parabolicity corrections to the electron band, or the loss of validity of both the effective-mass approximation and the Fröhlich continuum Hamiltonian for microstructures. Under the so-called *bulk phonon approximation*, and with the aforementioned simplifying assumptions, we provide a broad comprehensive version of the one-polaron problem, consisting of an electron confined within a deformable box that can be adapted into any desired geometric configuration.

2. Theory

2.1. The Hamiltonian

Using units appropriate to a polaron calculation ($m^\star = \hbar = \omega_{\mathrm{LO}} = 1$), the Hamiltonian describing the confined electron coupled to LO phonons is given by

$$H = H_{\mathrm{e}} + \sum_{Q} a_Q^\dagger a_Q + H_{\mathrm{e-ph}} \tag{1}$$

where

$$H_{\mathrm{e}} = \frac{1}{2}p^2 + V_{\mathrm{conf}}(\varrho, z) \tag{2}$$

is the electron part, with $V_{\mathrm{conf}}(\varrho, z)$ denoting the confining potential, and

$$H_{\mathrm{e-ph}} = \sum_{Q} V_Q (a_Q \mathrm{e}^{\mathrm{i}\boldsymbol{Q}\cdot\boldsymbol{r}} + \mathrm{HC}) \tag{3}$$

is the Fröhlich Hamiltonian. In the above, a_Q ($a_Q^\dagger$) is the phonon annihilation (creation) operator, $\boldsymbol{p}$ is the electron momentum, and $\boldsymbol{r} = (\boldsymbol{\varrho}, z)$ denotes the electron position in cylindrical coordinates. The interaction amplitude is related to the electron–phonon coupling constant α and the phonon wavevector $\boldsymbol{Q} = (\boldsymbol{q}, q_z)$ through $V_Q = (2\sqrt{2}\pi\alpha)^{1/2}/Q$.

To provide the confining potential, we adopt a three-dimensional box with adjustable parabolic barrier slopes, i.e., we set

$$V_{\mathrm{conf}}(\varrho, z) = \frac{1}{2}(\Omega_1^2\varrho^2 + \Omega_2^2 z^2) \tag{4}$$

in which the dimensionless frequencies Ω_i $(i = 1, 2)$ serve as the measures of the potential barrier strengths and the degree of confinement of the electron in the respective lateral (ϱ-) and $\pm z$-directions. By tuning Ω_1 and/or Ω_2 from zero to values much larger than unity, one can obtain a unified picture tracing the transition from the bulk to all of the possible extremes of the effective dimensionality—such as, for instance, to the two-dimensional slab-like confinement ($\Omega_1 = 0, \Omega_2 \gg 1$), or to the quasi-one-dimensional quantum well wire-like tubular geometry ($\Omega_1 \gg 1, \Omega_2 = 0$).

The rationale behind imposing quadratic potential profiles is that such a form for the confining barriers greatly facilitates the calculations, and leads to rather simple and tractable analytic expressions. We have thus refrained from treating potentials of other forms, which would possibly lead to complicated and even prohibitively difficult expressions and numerical complications, and yet would yield qualitative features similar to those for parabolic potential shapes. Indeed, calculations pertaining to the cyclotron study of polarons confined to an interface indicate that the phonon-coupling-induced shift in the resonant energy is sensitive predominantly to the strength of the confining potential, rather than its shape [8]. Besides this, the static depletion fields achieved in quantum wires and dots which are laterally confined by Schottky gates exhibit nearly parabolic potentials. We, therefore, reasonably use the parabolic confinement potential (4) to provide unified insight into the ground-state polaron properties in confined media, and a comprehensive review of the effect of confinement on the polaron binding in structures encompassing all geometric shapes of general interest.

2.2. Ground-state energy

In the Feynman path integral representation of the polaron, the phonon variables can be projected out exactly, to yield the partition function of the polaron in the form

$$\mathcal{Z}_{\rm pol} = \mathrm{Tr}\, \mathrm{e}^{-\beta H} = \mathcal{Z}_{\rm ph}\mathcal{Z} \tag{5}$$

where

$$\mathcal{Z}_{\rm ph} = \prod_{Q} \left[1 - \mathrm{e}^{-\beta}\right]^{-1} \tag{6}$$

is the phonon part, and

$$\mathcal{Z} = \int \mathcal{D}\boldsymbol{r}\ \mathrm{e}^{\mathcal{S}} \tag{7}$$

is the path integral in which the action $\mathcal{S}$ consists of two parts, one pertaining to the electron part of the Hamiltonian and the other to the electron–phonon interaction. In imaginary-time variables ($t \to -\mathrm{i}\lambda$), we have the expression

$$\mathcal{S} = \mathcal{S}_{\rm e} + \frac{1}{2}\sum_{Q} V_Q^2 \int_0^\beta \mathrm{d}\lambda \int_0^\beta \mathrm{d}\lambda'\ \mathrm{e}^{\mathrm{i}Q\cdot[\boldsymbol{r}(\lambda)-\boldsymbol{r}(\lambda')]} G_{(\omega_{\rm LO}=1)}(|\lambda - \lambda'|) \tag{8}$$

and

$$\mathcal{S}_{\rm e} = -\frac{1}{2}\int_0^\beta \mathrm{d}\lambda\ \left\{\dot{\boldsymbol{r}}^2(\lambda) + \Omega_1^2\varrho^2(\lambda) + \Omega_2^2 z^2(\lambda)\right\} \tag{9}$$

in which the dimensionless parameter β stands for the inverse temperature, and the memory function

$$G_\omega(u) = \frac{\cosh((\beta - 2u)\omega/2)}{\sinh(\beta\omega/2)} \quad \stackrel{\beta\to\infty}{\longrightarrow} \quad \mathrm{e}^{-\omega u} \tag{10}$$

is the Green's function of a harmonic oscillator with frequency ω. In principle, in the low-temperature limit, we have $\mathcal{Z}_{\rm pol} = \mathcal{Z}$, and the polaron ground-state energy

$$E_{\rm g} = -\lim_{\beta\to\infty} \beta^{-1} \log \mathcal{Z}$$

can be calculated exactly, provided that the path integral (7) can be evaluated. Since this is not possible due to the analytic complexity of the integral expressions in the action $\mathcal{S}$—equations (8) and (9)—we choose to proceed with the solvable trial action

$$\mathcal{S}_0 = \mathcal{S}_{\rm e} - \frac{w(v^2 - w^2)}{8} \int_0^\beta {\rm d}\lambda \int_0^\beta {\rm d}\lambda' \; [\boldsymbol{r}(\lambda) - \boldsymbol{r}(\lambda')]^2 G_w(|\lambda - \lambda'|) \tag{11}$$

which provides us with a convenient variational upper bound governed by the Jensen–Feynman inequality

$$E_{\rm g} \leqslant E_0 - \lim_{\beta\to\infty} \frac{1}{\beta} \langle \mathcal{S} - \mathcal{S}_0 \rangle_{\mathcal{S}_0} \tag{12}$$

where $\langle\ \rangle_{\mathcal{S}_0}$ denotes a path integral average with the density function $\mathrm{e}^{\mathcal{S}_0}$, and E_0 is the trial ground-state energy corresponding to $\mathcal{S}_0$. In equation (12), w and v are the variational parameters introduced within the same context as in the original paper by Feynman [5]. The problem then reduces to the evaluation of three quantities, E_0, A, and B, such that

$$E_{\rm g} = E_0 - B - A \tag{13}$$

is an upper bound, where the last two terms are given by

$$A = \lim_{\beta\to\infty} \frac{1}{2\beta} \sum_{\boldsymbol{Q}} V_{\boldsymbol{Q}}^2 \int_0^\beta {\rm d}\lambda \int_0^\beta {\rm d}\lambda' \; \left\langle \mathrm{e}^{\mathrm{i}\boldsymbol{Q}\cdot[\boldsymbol{r}(\lambda) - \boldsymbol{r}(\lambda')]} \right\rangle_{\mathcal{S}_0} G_{(\omega_{\rm LO}=1)}(|\lambda - \lambda'|) \tag{14}$$

$$B = \lim_{\beta\to\infty} \frac{1}{\beta} \frac{w(v^2 - w^2)}{8} \int_0^\beta {\rm d}\lambda \int_0^\beta {\rm d}\lambda' \; \left\langle [\boldsymbol{r}(\lambda) - \boldsymbol{r}(\lambda')]^2 \right\rangle_{\mathcal{S}_0} G_w(|\lambda - \lambda'|). \tag{15}$$

Since the trial action and the path integral averages involved in A and B are all separable in the Cartesian coordinates, the calculations can all be performed in an identical manner for each spatial direction. Denoting the Cartesian components of the electron position and momentum in any chosen direction by x and p_x, the corresponding Hamiltonian

$$H_0 = \frac{p_x^2}{2} + \frac{p_\phi^2}{2m_\phi} + \frac{1}{2}\Omega^2 x^2 + \frac{1}{2} m_\phi w^2 (x - \phi)^2 \tag{16}$$

(in which Ω stands for either Ω_1 or Ω_2) can be related to the one-dimensional analogue, $\mathcal{S}_0^{(1{\rm D})}$, of the trial action. Eliminating the harmonic oscillator variables ϕ and p_ϕ, one readily obtains

$$\mathcal{Z}_0 = \int \mathcal{D}x \;\; \exp\left[\mathcal{S}_0^{(1{\rm D})}\right] = 2\sinh\left(\frac{1}{2}\beta w\right) {\rm Tr}\, \mathrm{e}^{-\beta H_0} \tag{17}$$

and so

$$E_0^{(1{\rm D})} = \lim_{\beta\to\infty} -\frac{1}{\beta} \log \mathcal{Z}_0. \tag{18}$$

The Hamiltonian H_0, in which the term $\frac{1}{2}\Omega^2 x^2$ is the relevant part of the confining potential (4) along the chosen coordinate, describes the coupling of the harmonically confined electron to a fictitious particle of mass $m_\phi = (v^2 - w^2)/w^2$ which, in turn, gives the overall effect of the interaction of the electron with the phonon field (cf. figure 1).

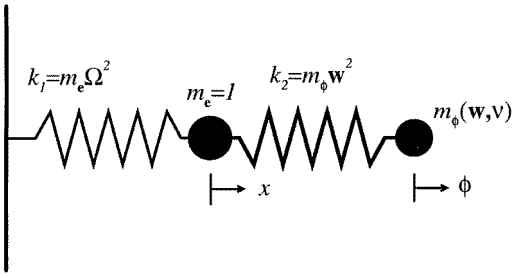

Figure 1. The coordinates and configuration of the coupled particles corresponding to $\mathcal{S}_0^{(1D)}$.

Under a suitable coordinate transformation

$$\begin{pmatrix} x \\ \phi \end{pmatrix} \to \begin{pmatrix} X \\ \Phi \end{pmatrix}$$

H_0 can be diagonalized in the normal coordinates X and Φ, yielding the eigenfrequencies

$$\begin{Bmatrix} \xi_1(\Omega) \\ \xi_2(\Omega) \end{Bmatrix} = \left\{ \frac{\Omega^2+\nu^2}{2} \mp \sqrt{\left(\frac{\Omega^2+\nu^2}{2}\right)^2 - \Omega^2 w^2} \right\}^{1/2} \tag{19}$$

in terms of which H_0 takes on the canonical form

$$H_0 = \frac{p_X^2}{2M} + \frac{p_\Phi^2}{2\mu} + \frac{1}{2}M\xi_1^2 X^2 + \frac{1}{2}\mu\xi_2^2\Phi^2 \tag{20}$$

where $M = \nu^2/w^2$ is sum of the mass of the electron and that of the fictitious particle. Using equations (17) and (18), the part of the ground-state energy contributed by the particular coordinate relevant to $\mathcal{S}_0^{(1D)}$ is obtained simply as

$$E_0^{(1D)} = \frac{1}{2}[\xi_1(\Omega) + \xi_2(\Omega) - w]. \tag{21}$$

Noting that the confinement potential $V_{\mathrm{conf}}(\varrho, z)$ is characterized by only two parameters, Ω_1 and Ω_2, the former governing the degree of localization of the electron in the lateral directions isotropically, and the latter relevant to the z-axis, the expression for $E_0^{(1D)}$ can be extended to account for each of the Cartesian coordinates all at once, yielding

$$E_0 = \sum_{n=1}^{2} \frac{1}{n}\left[\xi_1(\Omega_n) + \xi_2(\Omega_n) - w\right]. \tag{22}$$

Expanding the path integral average in the integrand in equation (14) up to order Q^2, i.e., writing

$$\left\langle \mathrm{e}^{\mathrm{i}\boldsymbol{Q}\cdot[\boldsymbol{r}(\lambda)-\boldsymbol{r}(\lambda')]} \right\rangle_{\mathcal{S}_0} \approx 1 + \mathrm{i}\boldsymbol{Q}\cdot\left\langle[\boldsymbol{r}(\lambda)-\boldsymbol{r}(\lambda')]\right\rangle_{\mathcal{S}_0} - \frac{1}{2}Q^2\left\langle[\boldsymbol{r}(\lambda)-\boldsymbol{r}(\lambda')]^2\right\rangle_{\mathcal{S}_0} \tag{23}$$

and using the integral transform

$$\int_0^\beta \mathrm{d}\lambda \int_0^\beta \mathrm{d}\lambda'\ F(|\lambda-\lambda'|) = \beta\int_0^\beta \mathrm{d}\eta\ F(\eta/2) \qquad (F(\beta-\eta)=F(\eta)) \tag{24}$$

the quantities A and B can be cast into more convenient forms. We obtain

$$A = \int_0^\infty \mathrm{d}\eta\ \mathrm{e}^{-\eta} \sum_Q V_Q^2\ \exp\left[-\frac{1}{2}\left(\frac{q^2}{\sigma_1(\eta)} + \frac{q_z^2}{\sigma_2(\eta)}\right)\eta\right]$$
$$= \frac{\alpha}{\sqrt{\pi}} \int_0^\infty \mathrm{d}\eta\ \mathrm{e}^{-\eta} \sqrt{\frac{\sigma_2(\eta)}{\eta}} \frac{\arctan\gamma}{\gamma} \tag{25}$$

where

$$\gamma = \left\{\frac{\sigma_2(\eta)}{\sigma_1(\eta)} - 1\right\}^{1/2} \tag{26}$$

and

$$B = \frac{w(v^2 - w^2)}{4} \int_0^\infty \mathrm{d}\eta\ \eta \mathrm{e}^{-w\eta}\left(\frac{2}{\sigma_1(\eta)} + \frac{1}{\sigma_2(\eta)}\right) = \sum_{n=1}^{2} \frac{1}{2n}\left[b_1(\Omega_n) + b_2(\Omega_n)\right]. \tag{27}$$

In the above, the parameters $\sigma_n(\eta)$ and $b_i(\Omega_n)$ ($n = 1, 2$ and $i = 1, 2$) are given by the following expressions:

$$\sigma_n(\eta) = \eta \left\{\sum_{i=1}^{2} \frac{d_i(\Omega_n)}{\xi_i(\Omega_n)}[1 - \mathrm{e}^{-\xi_i(\Omega_n)\eta}]\right\}^{-1} \tag{28}$$

with

$$d_i(\Omega_n) = \left\{1 + \frac{w^2(v^2 - w^2)}{[w^2 - \xi_i^2(\Omega_n)]^2}\right\}^{-1} \tag{29}$$

and

$$b_i(\Omega_n) = \frac{1}{w + \xi_i(\Omega_n)} \left\{\frac{1}{v^2 - w^2} + \frac{w^2}{[w^2 - \xi_i^2(\Omega_n)]^2}\right\}^{-1}. \tag{30}$$

2.3. The effective polaron mass

The variational model used in this work can be extended to yield the effective polaron mass in two distinctive geometric configurations, with either Ω_1 or Ω_2 set equal to zero. The extreme limits for which $\Omega_1 = 0$ and $\Omega_2 = 0$ or ∞ will be discussed in the next section.

We first refer to the quantum well slab-like geometry: $\Omega_1 = 0$. When the system is set in virtual motion with a small velocity, $\boldsymbol{u}_\varrho$, in the radial direction perpendicular to the z-axis, the total energy receives an additional kinetic contribution of the form

$$\delta K = \frac{1}{2} m_{\mathrm{p}}^{(\varrho)} u_\varrho^2$$

in which $m_{\mathrm{p}}^{(\varrho)}$ is to be identified as the polaron mass in the $\hat{\boldsymbol{\varrho}}$-direction. Imposing a virtual velocity in the theory is straightforward [5]. In section 2.1, the partition function $\mathcal{Z}$ has been written down for all of the paths with initial coordinate $\boldsymbol{r} = 0$ at time zero and final coordinate $\boldsymbol{r} = 0$ at the imaginary time β. With the virtual velocity $\boldsymbol{u}_\varrho$ turned on, the final coordinate should now be $\boldsymbol{r}(\beta) = \beta \boldsymbol{u}_\varrho$; and it is through this coordinate that one keeps track of the composite translational inertia of the coupled electron + phonon complex. We are thus encouraged to reformulate all of the terms in equation (13), where each of E_0, A, and B now becomes extended to a form consisting of a part relating to the ground-state energy of the polaron alone, and a part relating to the kinetic contribution which appears after we have imposed a virtual displacement on the polaron.

The additional kinetic extension involved in E_0 can be written readily as $\frac{1}{2}Mu_\varrho^2$, where M is the total mass (that of the electron and the fictitious particle), i.e., E_0 scales as

$$E_0 \to E_0 + \frac{1}{2}\frac{v^2}{w^2}u_\varrho^2. \tag{31}$$

For the remaining two quantities, A and B, we have the following modifications:

$$A \to \int_0^\infty \mathrm{d}\eta\ \mathrm{e}^{-\eta}\sum_{\boldsymbol{Q}} V_{\boldsymbol{Q}}^2 \exp\left\{-\frac{1}{2}\left(\frac{q^2}{\sigma_1(\eta)}+\frac{q_z^2}{\sigma_2(\eta)}\right)\eta + \mathrm{i}(\boldsymbol{q}\cdot\boldsymbol{u}_\varrho)\eta\right\} \tag{32}$$

and

$$B \to \frac{w(v^2-w^2)}{4}\int_0^\infty \mathrm{d}\eta\ \mathrm{e}^{-w\eta}\left[\left(\frac{2}{\sigma_1(\eta)}+\frac{1}{\sigma_2(\eta)}\right)+u_\varrho^2\eta^2\right] = B + \frac{1}{2}\frac{v^2-w^2}{w^2}u_\varrho^2. \tag{33}$$

Expanding equation (32) up to second order in $\boldsymbol{u}_\varrho$ (the first-order terms in $\boldsymbol{u}_\varrho$ vanish after one projects out the $\boldsymbol{Q}$-summation), and arranging the relevant terms in equation (13) to yield the form $E_\mathrm{g} \to E_\mathrm{g} + \delta K$, we obtain the following expression for the effective mass of the Q2D polaron in the slab geometry:

$$m_\mathrm{p}^{(\varrho)} = 1 + \frac{\alpha}{2\sqrt{\pi}}\int_0^\infty \mathrm{d}\eta\ \frac{\sqrt{\eta\sigma_2^3(\eta)}}{\gamma^2}\mathrm{e}^{-\eta}[\gamma^{-1}\arctan\gamma - (1+\gamma^2)^{-1}] \tag{34}$$

in which the variational parameters w and v have to be assigned their optimal-fit values, which minimize the ground-state energy with $\boldsymbol{u}_\varrho$ set equal to zero.

In order to calculate the mass in the relevant free direction in a quantum well wire tubular configuration, we follow the same steps in the formulation, but now $\boldsymbol{u}_\varrho$ is replaced by a virtual speed, u_z, along the z-axis. Consequently, the quantities E_0, A, and B are provided by the same expressions, equations (31)–(33), as were given for the slab geometry, except that all of the $\boldsymbol{u}_\varrho$ have to be replaced by u_z, and the product $\boldsymbol{q}\cdot\boldsymbol{u}_\varrho$ in equation (32) becomes $q_z u_z$. For the Q1D polaron mass we then obtain

$$m_\mathrm{p}^{(z)} = 1 + \frac{\alpha}{\sqrt{\pi}}\int_0^\infty \mathrm{d}\eta\ \frac{\sqrt{\eta\sigma_2^3(\eta)}}{\gamma^2}\mathrm{e}^{-\eta}[1-\gamma^{-1}\arctan\gamma]. \tag{35}$$

3. Results and conclusions

When $\Omega_i^{-1/2}$ ($i = 1$ and/or 2) is reduced to values comparable with the polaron size, the boundary effects start to become significant, and the system enters the regime of reduced dimensionality. Setting $\Omega_1 = 0$ and varying Ω_2 from zero to infinity, one can track the bulk polaron properties as they go over to those of a strictly 2D polaron. On the other hand, on deleting the confining potential along the z-axis ($\Omega_2 = 0$) and fixing Ω_1 at non-zero finite values, the theory reflects the Q1D description in a quantum well wire-like tubular structure. Hereafter, we will consider the polaron binding energy relative to the subband level as $\mathcal{E}_\mathrm{p} = \Omega_1 + \frac{1}{2}\Omega_2 - E_\mathrm{g}$, and use Ω to mean Ω_1 (Ω_2) when Ω_2 (Ω_1) $= 0$. In the spherically symmetric box-type configuration, we simply set $\Omega_1 = \Omega_2 = \Omega$. Similarly, we shall use $\sigma(\eta)$ to mean $\sigma_1(\eta)$ and/or $\sigma_2(\eta)$.

Since analytical minimization of E_g, equation (13), is not possible, the determination of the optimal fits to w and v, and the polaron quantities of interest, requires treatment on a computer. Before we present our numerical results over a broad range of the confining parameters and the coupling constant, we find it useful to investigate the conformity with a few extreme cases which have already been treated in the literature, and are well understood.

3.1. Integer-dimensional-space limits

Setting $\Omega_1 = 0$ and $\Omega_2 = 0$ or ∞, we attain respectively the bulk (3D) and strictly two-dimensional (2D) limits, where the general expressions (22), (25), (27) and (34), (35) for the ground-state energy and mass take on more tractable and simple forms. For $\Omega_1 = \Omega_2 = 0$, the theory duplicates the results of the original paper by Feynman [5]. In this limit the eigenfrequencies (19) reduce to $\xi_1(0) = 0$ and $\xi_2(0) = v$, and we obtain

$$\sigma(\eta) = \left\{ \frac{w^2}{v^2} + \left(1 - \frac{w^2}{v^2}\right) \frac{1 - \mathrm{e}^{-v\eta}}{v\eta} \right\}^{-1} \tag{36}$$

$$E_0 = \frac{3}{2}(v - w) \tag{37}$$

$$B = \frac{3}{4}(v^2 - w^2)/v \tag{38}$$

yielding the binding energy

$$\mathcal{E}_\mathrm{p} = -E_\mathrm{g} = A - \frac{3(v - w)^2}{4v} \tag{39}$$

where

$$A = \frac{\alpha}{\sqrt{\pi}} \int_0^\infty \mathrm{d}\eta \ \mathrm{e}^{-\eta} \sqrt{\frac{\sigma(\eta)}{\eta}}. \tag{40}$$

Furthermore, from equation (34) we obtain that the 3D (isotropic) mass is given by

$$m_\mathrm{p} = 1 + \frac{\alpha}{3\sqrt{\pi}} \int_0^\infty \mathrm{d}\eta \ \mathrm{e}^{-\eta} \sqrt{\eta \sigma^3(\eta)}. \tag{41}$$

Going over to the strict 2D characterization of the polaron, we have

$$\lim_{\Omega_2 \to \infty} \begin{Bmatrix} \xi_1(\Omega_2) \\ \xi_2(\Omega_2) \end{Bmatrix} = \begin{Bmatrix} w \\ \infty \end{Bmatrix} \tag{42}$$

and, consequently, $\sigma_1(\eta) = \sigma(\eta)$ as given in equation (36), and $\sigma_2(\eta) \to \infty$. For the 2D binding energy we then obtain [9]

$$\mathcal{E}_\mathrm{p} = -\left(E_\mathrm{g} - \frac{1}{2}\Omega_2\right) = A - \frac{(v - w)^2}{2v} \tag{43}$$

in which A is provided by the same expression, equation (40), as was given for the bulk case, except that the coefficient multiplying the η-integral is now $(\sqrt{\pi}/2)\alpha$. Similarly, the 2D polaronic mass is given by equation (41), where the corresponding factor multiplying the η-integral scales to $(\sqrt{\pi}/4)\alpha$.

For an extensive treatment of the polaron problem in (integer) N dimensions, the reader is referred to reference [10]. Here (cf. figure 2), we shall be content to just present numerical displays of the variational parameters w and v, the binding energy, and the polaron mass for $N = 3$ and $N = 2$ over a wide range of the coupling constant encompassing the weak- and the strong-coupling extremes.

3.2. The weak-coupling limit

Since in the most commonly studied compound semiconductors the electron–phonon coupling is rather weak, we would like to place particular emphasis on the weak-coupling regime. A discussion of the present model within the perturbation approach has already been provided in reference [7], with which we wish to establish some correspondence here.

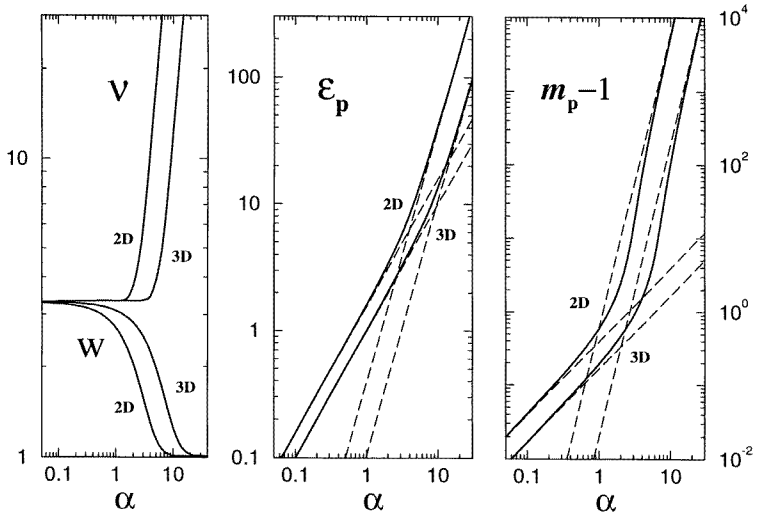

Figure 2. The variational parameters w and ν, the binding energy, and the mass for three- and two-dimensional polarons as functions of the coupling constant. The dashed lines relate to the perturbation and strong-coupling theories.

For weak coupling, the parameters w and ν tend asymptotically to the same constant value ($\approx$3.3), while preserving the intrinsic relation $\nu > w$ (cf. reference [5]), and in the limit $\alpha \to 0$, one has $\nu - w = \mathcal{O}(\alpha)$ regardless of the degree of confinement. Hence, setting $\nu \approx w$, we have

$$\left\{ \begin{matrix} \xi_1(\Omega) \\ \xi_2(\Omega) \end{matrix} \right\} \approx \left\{ \frac{\Omega^2 + w^2}{2} \mp \frac{|\Omega^2 - w^2|}{2} \right\}^{1/2} \tag{44}$$

yielding the simplifications $E_0 = \Omega_1 + \frac{1}{2}\Omega_2$ and $B = 0$. In the weak-α regime, we thus readily establish that the binding energy is given solely by A, equation (25), wherein $\sigma_{n=1,2}$, equation (28), reduces to exactly the same expression as was derived previously within the framework of second-order perturbation theory [7], i.e.,

$$\sigma_n(\eta) = \frac{\Omega_n \eta}{1 - \mathrm{e}^{-\Omega_n \eta}} \qquad n = 1, 2. \tag{45}$$

An elaborate study of the weak-coupling polaron quantities as functions of Ω_1 and Ω_2 can be found in reference [7]. We therefore do not repeat the relevant results here, and readdress only the three- and two-dimensional limits. In approaching the bulk case, we assume a spherically symmetric isotropic confinement: $\Omega_1 = \Omega_2 = \Omega \ll 1$, and for the 2D limit we set $\Omega_1 = 0$, and let $\Omega_2 = \Omega \gg 1$. From equations (13) and (34), we derive the binding energy and the polaron mass up to the lowest-order contribution from Ω as follows:

$$\mathcal{E}_\mathrm{p} = \begin{cases} \lim\limits_{\Omega \to 0} \alpha \left(1 + \dfrac{\Omega}{8} \right) & \text{3D} \\ \lim\limits_{\Omega \to \infty} \dfrac{\pi}{2} \alpha \left(1 - \dfrac{4}{\sqrt{\Omega}} \right) & \text{2D} \end{cases} \tag{46}$$

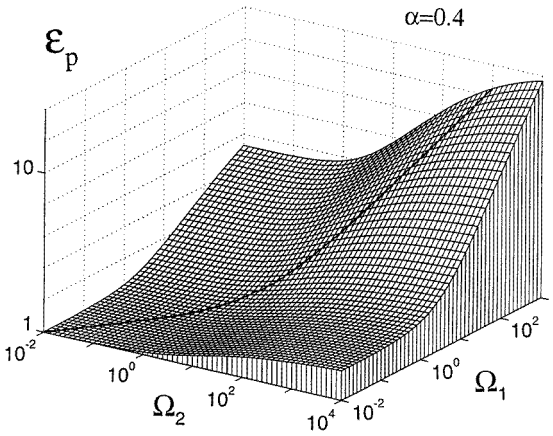

Figure 3. The binding energy (scaled relative to the bulk value) as a function of the confining parameters for weak coupling ($\alpha = 0.4$). The diagonal curve on the grid refers to the spherically symmetric configuration ($\Omega_1 = \Omega_2$).

$$m_{\mathrm{p}} = \begin{cases} \lim\limits_{\Omega\to 0} 1 + \dfrac{1}{6}\alpha\left(1 + \dfrac{9}{8}\Omega\right) & \text{3D} \\ \lim\limits_{\Omega\to\infty} 1 + \dfrac{\pi}{8}\alpha\left(1 - \dfrac{4}{\sqrt{\pi^3\Omega}}\right) & \text{2D.} \end{cases} \tag{47}$$

3.3. The overall view

For a complete description covering the ranges between all possible extremes of the effective dimensionality and the coupling constant, we refer back to the set of equations (22), (25), and (27), and numerically minimize the ground-state energy (13) with respect to the variational parameters w and v. In figure 3 we select $\alpha = 0.4$ (appropriate for CdTe), and construct a unified physical image of the polaron binding over a reasonably broad range of Ω_1 and Ω_2, covering all of the interesting regimes of the effective dimensionality. Starting from the flat plateau at the bottom (corresponding to the bulk case), and following the incline for increasing values of Ω_2, one arrives at a second plateau characterizing the two-dimensionally confined nature of the polaron. On following the direction parallel to the Ω_1-axis, however, $\mathcal{E}_{\mathrm{p}}$ is seen to increase steadily at a much faster rate, and rapidly become much larger than in the Q2D configuration, which follows essentially from the fact that, in the wire geometry, the polaron becomes highly localized towards the wire axis, due to confinement arising from all transverse directions. For instance, for the Q2D confinement with $\Omega = 10$, we find $\mathcal{E}_{\mathrm{p}}$ to be 1.16 times its bulk value, $\mathcal{E}_{\mathrm{p}}^{(3\mathrm{D})}$. For the case of a wire with the same parameter value, the binding becomes stronger by an even greater factor of about 1.45 than the 3D energy. On lowering the dimensionality one step further down, to the spherically symmetric quantum well box-type localization of the polaron (displayed by the diagonal curve on the grid in figure 3), the effective electron–phonon coupling is observed to be even stronger ($\mathcal{E}_{\mathrm{p}}/\mathcal{E}_{\mathrm{p}}^{(3\mathrm{D})} = 2.02$), since now the polaron becomes radially squeezed in all directions. The corresponding values when Ω is set to 10^2 are 1.34, 2.27, and 5.70.

For completeness, we extend our considerations to the regime of strong phonon coupling, and, in figure 4, with the confining parameter held fixed ($\Omega = 10^2$), we plot profiles of the polaronic binding as a function of growing α for the quasi-two-, quasi-one-, and quasi-

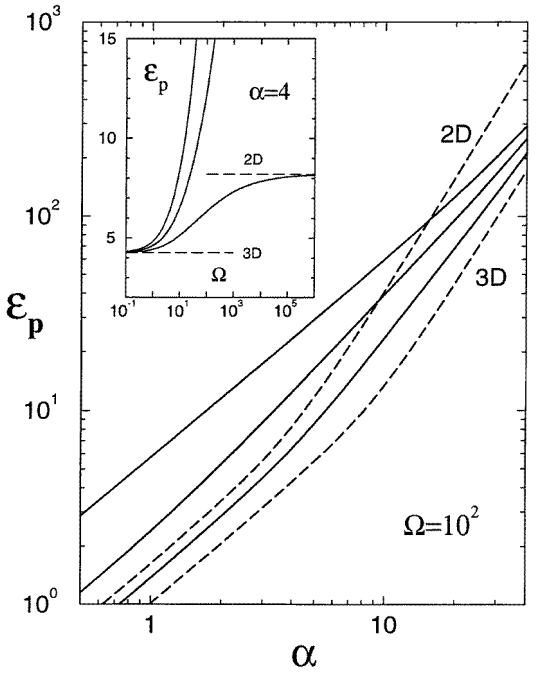

Figure 4. The binding energy as a function of the coupling constant with Ω ($=\Omega_1$ and/or Ω_2) held fixed. The solid curves from bottom to top are respectively for the quasi-two-, quasi-one-, and quasi-zero-dimensional configurations, and the dashed curves give the bulk and strictly 2D polaron energies. The inset provides an alternative view of the binding energy as a function of Ω, in the strong-coupling regime.

zero-dimensional configurations, thus providing a comparison of the binding energy values for a succession of effective dimensionalities pertaining to the slab-, wire-, and box-type geometries. The inset in the figure gives a complementary display of $\mathcal{E}_p$ as a function of Ω, where the coupling constant has been selected arbitrarily to be an order of magnitude larger than for CdTe. The general trend towards the electron–phonon coupling being inherently stronger in reduced dimensionalities is seen to be reflected in the plots which we have generated so far.

It should be mentioned that the parameters α and Ω ($=\Omega_1$ or Ω_2) characterizing the model do not enter the problem in an independent way, but together take part in a linked manner in the binding and act collaboratively in favour of stronger binding. Thus, a high degree of localization in cases of reduced dimensionality is expected to lead to a pseudo-enhancement of the effective electron–phonon coupling. Even for weak coupling ($\alpha \ll 1$), when the polaron is in a delocalized state with a large spread, the influence of the geometric confinement on the polaron is immediate when Ω is turned on, and, to first order in small Ω, the coupling constant is observed to scale as $\alpha \to \alpha[1 + \mathcal{O}(\Omega)]$ (cf. equations (46) and (47), for instance).

For $\alpha \gg 1$, however, the situation is somewhat different. In this extreme, the polaron is already in a highly localized state, and a small-sized polaron is not expected to feel the effect of the confining boundary, except for very large Ω. This peculiar aspect can be seen clearly if the energy and mass of the confined polaron are displayed relative to their corresponding bulk values, $\mathcal{E}_p^{(3D)}$ and $m_p^{(3D)}$. For this purpose, we choose to refer to the slab

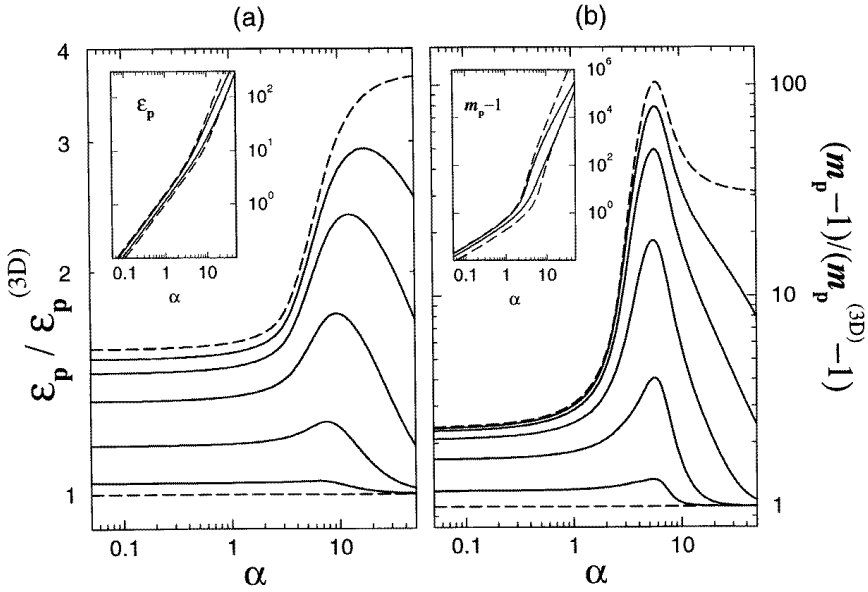

Figure 5. (a) The binding energy, and (b) the polaron mass, as functions of the coupling constant in the quasi-two-dimensional configuration. All of the energy and mass values (except those in the insets) are scaled relative to the corresponding bulk values. The solid curves (from bottom to top) constrained by the lower (3D) and upper (2D) dashed curves are, respectively, for $\Omega \equiv \Omega_2 = 1, 10, 10^2, 10^3,$ and 10^4. Similarly, the solid curves in the insets are for $\Omega = 10$ and 10^3.

configuration, and portray (cf. figure 5) the variations of the binding energy and the mass (along the relevant free direction) as functions of the electron–phonon coupling strength for a succession of different Ω values. In view of our results plotted in the figure, we see that, starting from the weak-coupling extreme, the growth rates (with respect to α) of the binding energy and mass in low-dimensional configurations ($\Omega > 0$) are not significantly different from that for the bulk polaron. However, as α is tuned to greater values, the polaron goes into a more deeply bound state, and, under the additional spatial constraint confining it, the binding becomes even deeper, since now the intrinsic collaborative role which the geometric confinement plays in the effective phonon coupling becomes much more effective and prominent. In the meantime, contrary to this trend, with growing α the polaron becomes substantially localized, and becomes unaffected by the boundary potential, except for large values of Ω—thus leading to a partial reduction in the confinement counterpart of the polaron binding. Clearly, in the extreme limit of an artificially large α dominating over the external confinement, the problem should be characterized essentially by its bulk description. This salient feature is manifested in the plots for finite Ω by the fact that the energy and mass profiles, after having each displayed a maximum, start to fall off, and eventually match their bulk values as α is made stronger. A complementary remark that we might make in this regard is that, for a large Ω, one requires a correspondingly large α for the polaron to conform to its bulk characterization, and, in particular, in the strict 2D limit ($\Omega \to \infty$) of the slab-like confinement, one should correspondingly have $\alpha \to \infty$. This feature can readily be seen from the fact that the upper dashed curves in the figure tend to the two-dimensional limiting values, $3\pi^2/8$ and $81\pi^4/256$, for the energy and mass, respectively.

In this article we have uncovered the fundamental aspects of the polaron problem in a confined medium within a unified scheme encompassing the bulk and all low-dimensional geometric configurations of general interest. The Feynman path integral theory adapted to the 'deformable potential box' model allows us to achieve a simple and yet comprehensive review of the ground-state polaron properties of structures with reduced dimensionality.

References

[1] Das Sarma S and Mason B A 1985 *Ann. Phys., NY* **163** 78
[2] Peeters F M and Devreese J T 1987 *Phys. Rev.* B **36** 4442
[3] Degani M H and Hipólito O 1988 *Solid State Commun.* **65** 1185
[4] Erçelebi A and Senger RT 1996 *Solid State Commun.* **97** 509
[5] Feynman R P 1955 *Phys. Rev.* **97** 660
[6] Yıldırım T and Erçelebi A 1991 *J. Phys.: Condens. Matter* **3** 1271
[7] Yıldırım T and Erçelebi A 1991 *J. Phys.: Condens. Matter* **3** 4357
[8] Larsen D M 1985 *Proc. 17th Int. Conf. on the Physics of Semiconductors* ed J D Chadi and W Harrison (Berlin: Springer) p 421
[9] Wu Xiaoguang, Peeters F M and Devreese J T 1985 *Phys. Rev.* B **31** 3420
[10] Peeters F M, Wu Xiaoguang and Devreese J T 1986 *Phys. Rev.* B **33** 3926